Design and use of multisine signals for Li-ion battery equivalent circuit modelling. Part 2: Model estimation

W.D. Widanage[a,*], A. Barai[a], G. H. Chouchelamane[b], K. Uddin[a], A. McGordon[a], J. Marco[a], P. Jennings[a]

[a] *WMG, University of Warwick, Coventry. CV4 7AL. U.K.*
[b] *Jaguar Land Rover, Banbury Road, Warwick. CV35 0XJ. U.K.*

Abstract

An Equivalent Circuit Model (ECM) of a lithium ion (Li-ion) battery is an empirical, linear dynamic model and the bandwidth of the input current signal and level of non-linearity in the voltage response are important for the model's validity. An ECM is, however, generally parametrised with a pulse current signal, which is low in signal bandwidth (Part 1) and any non-linear dependence of the voltage on the current due to transport limitations is ignored. This paper presents a general modelling methodology which utilises the higher bandwidth and number of signal levels of a pulse-multisine signal to estimate the battery dynamics and non-linear characteristics without the need of a 3D look-up table for the model parameters. In the proposed methodology a non-parametric estimate of the battery dynamics and non-linear characteristics are first obtained which assists in the model order selection, and to assess the level of non-linearity. The new model structure, termed as the Non-linear ECM (NL-ECM), gives a lower Root Mean Square

*Corresponding author. Email: Dhammika.Widanalage@warwick.ac.uk. Address: WMG, University of Warwick, Coventry, CV4 7AL, UK. Telephone: 0044 24765 28191.

(RMS) and peak error when compared to an ECM estimated using a pulse data set.
Keywords: Multisine signals, Drive-cycle, Li-ion battery, Equivalent Circuit Modelling, Sigmoid function

---

Abbreviations

BMS Battery Management System

DFT Discrete Fourier Transform

ECM Equivalent Circuit Model

EIS Electrochemical Impedance Spectroscopy

EV Electric Vehicle

FFT Fast Fourier Transform

LPM Local Polynomial Method

NCA Nickel Cobalt Aluminium oxide

NL-ECM Non-linear Equivalent Circuit Model

OCV Open-circuit-voltage

pk-error Peak error

PPC Pulse Power Current

RMSE Root Mean Square Error

SoC State-of-Charge

Notations

A_k : Amplitude of the k^{th} multisine harmonic

α : Scale factor for smallest base-signal pulse $0 < \alpha < 1$

C_1 : C-rate of largest pulse in the base-signal

C_2 : C-rate of smallest pulse in the base-signal

C_{cmax} : Maximum applicable 10s charge C-rate

C_{dmax} : Maximum applicable 10s discharge C-rate

$\boldsymbol{C}_{\hat{\boldsymbol{\theta}}}$: Estimated covariance matrix of parameter vector $\boldsymbol{\theta}$

$\boldsymbol{E}$: Error vector when estimating the impedance via the LPM

η : Over-potential (V)

F : Highest excited multisine harmonic number

f_s : Sampling frequency (Hz)

γ : Scale factor for largest base-signal pulse $0 < \gamma < 1$

H_{exc} : Set of excited multisine harmonics

$I(k)$: DFT of $\bar{i}(n)$ at harmonic k

$i(n)$: Sampled current signal (A)

$\bar{i}(n)$: Sampled current signal averaged over periods (A)

i_d : Current density (A.cm^{-2})

$\boldsymbol{K}$: Regressor matrix when estimating the impedance via the LPM

$L[\bullet]$: A linear transform operator

N : Number of samples per period of the multisine signal

ω_k : Discrete angular frequency $\omega_k = 2\pi k f_s/N$ (rad.s^{-1})

P : Number of applied pulse-multisine periods

ϕ_k : Phase of the k^{th} multisine harmonic

S : Polynomial order of the LPM

$\sigma_{\hat{Z}}(k)$: Estimated standard deviation of impedance at harmonic k

T_1 : Time interval of largest base-signal pulse (s)

T_2 : Time interval of first rest period in the base-signal (s)

T_4 : Time interval of last rest period in the base-signal (s)

$\boldsymbol{\theta}$: Parameter vector when estimating the impedance via the LPM

$V(k)$: DFT of $\bar{v}_0(n)$ at harmonic k

$v(n)$: Sampled voltage signal (V) sort

$\bar{v}_0(n)$: Over-voltage signal averaged over periods (V) sort

$\bar{v}(n)$: Sampled voltage signal averaged over periods (V)

$v_l(n)$: Simulated linear over-voltage signal (V)

$\bar{v}_l(n)$: Simulated linear over-voltage signal averaged over periods (V)

$Z(k)$: Impedance at harmonic k

$Z_m(k)$: Transfer function model evaluated at harmonic k

$\hat{Z}(k)$: Estimated impedance at harmonic k

1. Introduction

Part 1 of this paper series demonstrated that the bandwidth of a Pulse Power Current (PPC) test is limited to around 100mHz (for a 10 second pulse), which is lower than that of a drive-cycle signal. Additionally a new signal design technique to generate a more realistic current signal known as a pulse-multisine was presented [1]. A pulse-multisine is a signal with characteristics resembling the bandwidth of a drive cycle and the signal spans the full applicable current range of a battery. Part 1 discussed how the increased bandwidth, periodicity and high number of signal levels of a pulse-multisine are advantageous for modelling battery dynamics. These properties are used to present a new modelling methodology and model structure for lithium ion (Li-ion) battery dynamics appropriate for use in a Battery Management System (BMS).

The development and use of a Li-ion battery model is motivated by its application. A BMS in an Electric (EV) or a Hybrid Electric Vehicle (HEV) is one such application which relies on an accurate battery model to assess the battery pack health and power delivering capabilities [**?**]. With the battery current assumed as the independent variable the model should accurately predict the voltage response given the initial states of the battery. This mapping from current to voltage has been realised extensively in the form of an Equivalent Circuit Model (ECM) [2, 3, 4, 5]. Models that do not rely on the current to voltage causality have also been developed in [6], and in [7] a Li-ion Bond Graph model is presented.

The success of the ECM is due to the limited number of model parameters required and the ease of simulation. The type of test data typically used for an ECM parametrisation include Open-Circuit-Voltage (OCV) measurements and PPC or Electrochemical Impedance Spectroscopy (EIS) frequency data. The OCV data is used to characterise the thermodynamic potential and hysteresis of a Li-ion battery and the PPC or EIS data are used to model the potential drops due to Ohmic losses, charge-transfer kinetics, double layer effect and mass transport [8].

PPC tests are recorded at different SoC and temperatures allowing a range of ECM parameters to be estimated, and when in simulation be interpolated (via a 2D look-up table), over the range of SoC and temperatures values [9, 10, 11]. Furthermore, by estimating two separate sets of ECM parameters for charge and discharge the model fidelity can be increased to include SoC, temperature and current direction (charge or discharge) [12].

At lower temperatures ($\leq$ 10 °C) and high C-rates, however, ion trans-

port diffusion limitations can occur [8]. This leads to a non-linear dependence of the voltage on the current. The ECM parameters should therefore also be a function of current magnitude or C-rate and as well as temperature. In [13] an ECM is estimated whereby the circuit parameters for each of the PPC pulses are included in a 3D look-up table for interpolation and simulation.

A 3D look-up table, however, requires that the ECM parameters are available for each combination of current, SoC and temperature. This requirement imposes practical difficulties since at lower temperatures the increase in internal resistance will not permit all of the standard PPC current pulses to be applied as the battery voltage reaches its minimum and maximum cut-off limits. As such the current dependence of the ECM parameters via a look-up table is usually omitted and only characterised as a function of current direction, SoC and temperature.

In this paper a new modelling methodology is presented to estimate a non-linear ECM (NL-ECM). The NL-ECM consists of a linear ECM and a non-linear over-voltage function. The linear ECM captures the Li-ion battery kinetics (internal resistance and charge transfer dynamics) and the non-linear over-voltage function captures the non-linear dependence of the voltage on the current due to diffusion limitations without the need of a 3D lookup table. To parametrise the linear ECM the voltage response based on a pulse-multisine [1] at a particular SoC and temperature is used to estimate the battery impedance, which in turns allows an appropriate ECM model order to be estimated. The large number of C-rates of a pulse-multisine, as opposed to a few distinct C-rates of a PPC, is then used to characterise the non-linear over-voltage function.

The methodology however still requires OCV data to characterise the thermodynamic voltage and battery hysteresis. It is shown that the new model structure together with the pulse-multisine signal lead to a reduction of the model root mean square error (RMSE) and peak error when compared to a linear ECM estimated with PPC data. The procedure therefore combines the advantages of a pulse-multisine signal, which includes a considerable reduction in experimental time (to several minutes) per SoC and temperature, and estimate a more accurate model over the bandwidth of interest for a BMS.

Part 2 of this paper series is structured as follows, in Section 2 the battery and experiment details for the model development are described. Sections 3 and 4 give an explain of model estimation and validation and in Sections 5 and 6 model complexity and the main conclusions of the modelling procedure are discussed.

2. Experiment details

In this work the current to voltage relationship of four 18650 3.03Ah $LiNiCoAlO_2$ (NCA) batteries are modelled using pulse-multisine current signals. Similar to a PPC test procedure where the model parameters are obtained over different SoCs and temperatures, a pulse-multisine is applied at five SoCs which were $10\%, 20\%, 50\%$, 80% and 95% and at four temperatures 0 °C , 10 °C , 25 °C and 45 °C to parametrise the model.

The maximum applicable 10 s discharge/charge current (C_{dmax} and C_{cmax}) is known from the battery specifications. As such the five design parameters of the pulse-multisine are, α the scale factor, T_1, T_2, T_4 the time interval of

the largest pulse and two rest periods respectively and H_{exc} the excitation bandwidth of the random phase multisine, as described in Part 1 of this series, were set for each SoC and temperature. These parameter values are given in Table A.2.

In all cases the sampling frequency was set to $f_s = 10$ Hz and the maximum harmonic in H_{exc} was selected to span a bandwidth of at most 1Hz. Five periods (let P denote number of periods) of the designed pulse-multisine (denoted as $i(n)$) were applied and the corresponding voltage response (denoted as $v(n)$) was measured. The number of periods is selected such that the battery dynamics reach steady-state while limiting the surface temperature increase to approximately 2-3 °C . Through several experiment runs five periods were found sufficient to fulfil both criteria. Figure 1 shows an example of five periods of the current pulse-multisine and voltage response measured at 20 % SoC and 45°C .

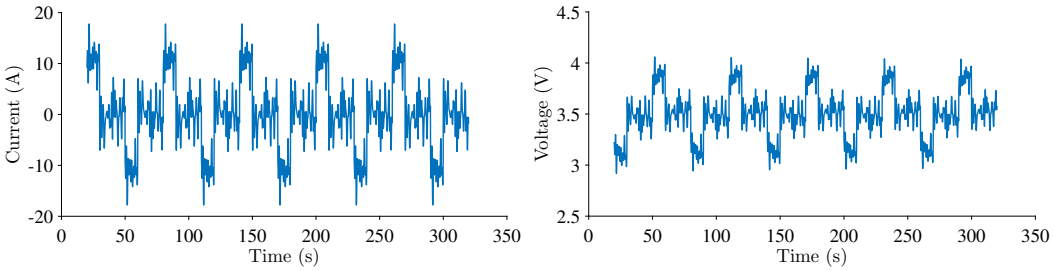

(a) Five periods of the pulse-multisine current (b) Five periods of the voltage response

Figure 1: Five periods ($P = 5$) of the pulse-multisine current and voltage response at 20 % SoC 45 °C of a 18650 Li-ion NCA battery.

3. Model estimation

As current is the controlled variable in the experiments the development of a current input model is described in this section. The NL-ECM model consists of three elemental blocks which includes a linear ECM, a nonlinear over-voltage function $f(v_l)$ and an OCV coupled with hysteresis block (Figure 2).

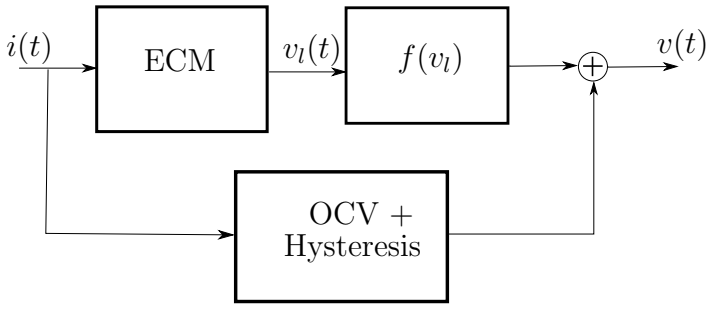

Figure 2: Li-ion battery NL-ECM structure. The overall model consists of a linear ECM followed by a non-linear over-voltage function and a parallel OCV and hysteresis model block.

The following subsections describes the identification of the corresponding model blocks.

3.1. Impedance estimate and equivalent circuit transfer function

The typical approach for estimating an ECM is to directly fit or optimise the model parameters based on the measured current and voltage data set (normally a PPC data set). Doing so, however, requires a prior assumption of an ECM model structure. In this paper an intermediate step is performed whereby the battery impedance, which is a non-parametric estimate of the battery dynamics, and its standard deviation are first estimated. This

impedance estimate will assist in deciding an appropriate ECM model order and structure in the form of a transfer function which can be fitted to obtain the ECM model parameters.

As impedance is defined under steady-state conditions, to reduce the influence of any transient behaviour, the first period of the measured voltage and current is discarded when estimating the impedance. The remaining $P-1$ periods are then averaged over periods as

$$\bar{i}(n) = \frac{1}{P-1}\sum_{p=2}^{P} i(N(p-1)+n), \quad \bar{v}(n) = \frac{1}{P-1}\sum_{p=2}^{P} v(N(p-1)+n)$$
$$n = 0, \ldots, N-1 \quad (1)$$

In equation (1) N is the number of samples per period of the applied pulse-multisine.

The mean voltage around which the voltage measurements are made is then removed from $\bar{v}(n)$ prior to estimating the impedance and will subsequently be accounted for by the OCV and hysteresis model block. The resulting zero-mean voltage, denoted as $\bar{v}_0(n)$, is defined in this work as the *over-voltage* signal and is

$$\bar{v}_0(n) = \bar{v}(n) - \frac{1}{N}\sum_{n=0}^{N-1} \bar{v}(n) \quad (2)$$

The Discrete Fourier Transform (DFT) of $\bar{i}(n)$ (the averaged current signal) and $\bar{v}_0(n)$ (the over-voltage signal) is then computed as

$$I(k) = \sum_{n=0}^{N-1} \bar{i}(n)e^{-2j\pi kn/N}, \quad V(k) = \sum_{n=0}^{N-1} \bar{v}_0(n)e^{-2j\pi kn/N}$$
$$k = 0, \ldots, N-1 \quad (3)$$

where $I(k)$ and $V(k)$ in equation (3) denote the DFT of $\bar{i}(n)$ and $\bar{v}_0(n)$ at the k^{th} harmonic.

The DFT voltage is related to the DFT current through the product with the battery impedance (equation (4)).

$$V(k) = Z(k)I(k) + E(k) \tag{4}$$

$Z(k)$ is the impedance which is to be estimated and $E(k)$ is an error term accounting for any measurement error and for any error arising from non-linear battery behaviour.

In order to estimate $Z(k)$, given $I(k)$ and $V(k)$, the influence of the error term should be minimised (typically in a least squares sense). A procedure known as the local-polynomial method (LPM) is used in this work which allows for both the impedance and standard deviation to be estimated. Details on the LPM are found in [14] while a brief description of the procedure is presented in Appendix B.

The estimated impedance (magnitude and phase) and standard deviation of the battery when at 20 % and 45 °C is shown in Figure (3). The magnitude response (3a) of the impedance has an increasing gain at low frequencies and the phase response (3b) approaches 180° as the frequency increases. Such a response can be attributed to mass transport from diffusion at low (≤ 1 Hz) frequencies [8].

When fitting a transfer function to the impedance, the increase in low frequency magnitude indicates the presence of a pole[1] close to the origin in the complex domain. The phase approach to 180° indicates a transfer

[1] A pole is defined as a root of the transfer function denominator

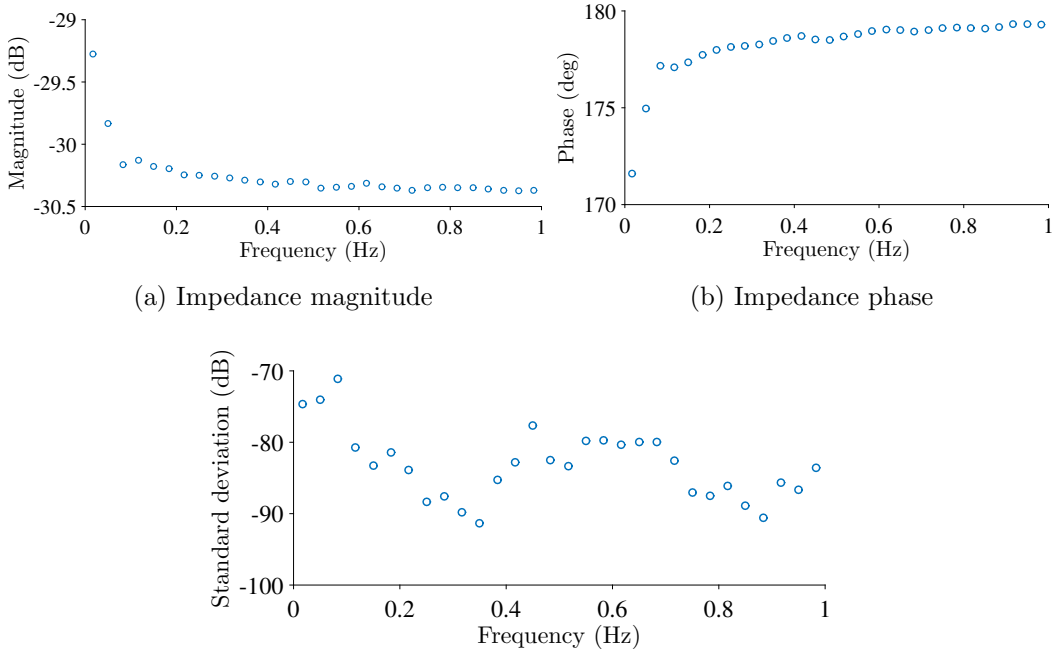

(a) Impedance magnitude

(b) Impedance phase

(c) Impedance standard deviation

Figure 3: Estimated impedance and standard deviation at 20 % SoC 45 °C of a 18650 Li-ion NCA battery.

function with a negative gain factor and an equal numerator and denominator polynomial degree of the form

$$Z_m(k) = -\left(\frac{b_{nb}(j\omega_k)^{nb} + \cdots + b_1 j\omega_k + b_0}{(j\omega_k)^{nb} + \cdots + a_1 j\omega_k + a_0}\right) \tag{5}$$

In equation (5) $Z_m(k)$ denotes the transfer function model, where $\omega_k = 2\pi k f_s/N$ is the discrete angular frequency at harmonic k and nb is the model order.

For a given model order the transfer function coefficients are estimated by minimising a cost-function (J) and is defined as the sum of the weighted squared errors between the estimated impedance and the transfer function

model.

$$J = \sum_{k \in H_{exc}} \left| \frac{Z(k) - Z_m(k)}{\sigma_{\hat{Z}}(k)} \right|^2 \tag{6}$$

In equation (6) $\sigma_{\hat{Z}}(k)$ is the estimated standard deviation of the impedance and is the first diagonal entry of the estimated covariance matrx $\boldsymbol{C}_{\hat{\boldsymbol{\theta}}}$ (equation (B.5)). For this optimisation the Frequency Domain System Identification Toolbox in Matlab® is used [15], to which the estimated impedance and standard deviation are passed along with a transfer function order as function arguments.

Figure 4 shows a 1st and 2nd order fit of the impedance and the cost function for the two models are $J = 638.0$ and $J = 56.4$ respectively. Using

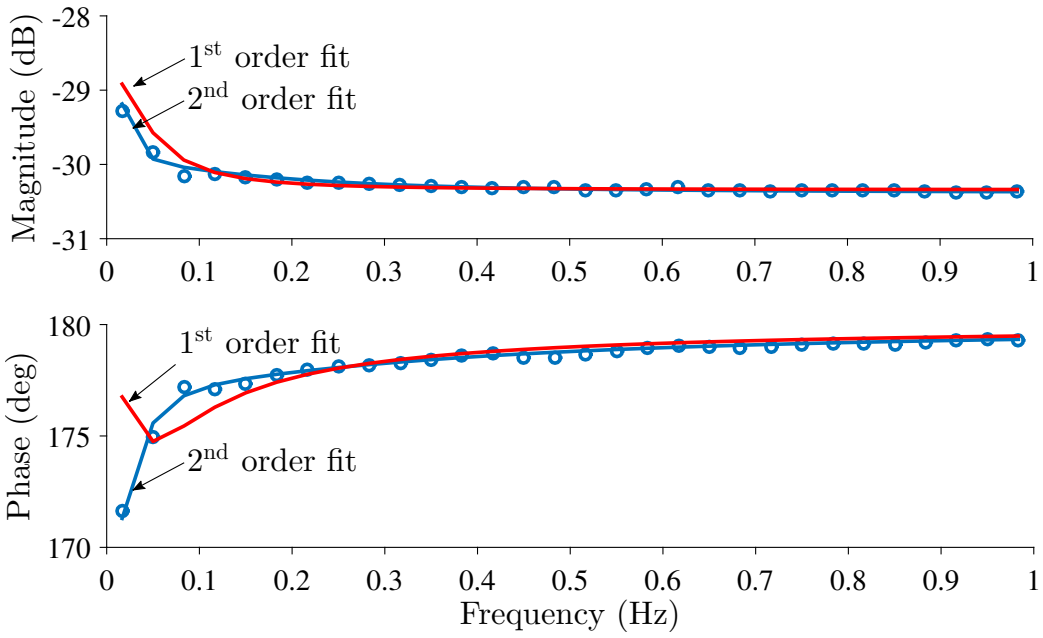

Figure 4: A 2nd order transfer function gives a better fit than a 1st order transfer function. Fit shown for impedance estimated at 20 % SoC and 45 °C of a 18650 Li-ion NCA battery.

orders greater than two generally improved the fit, however, this improvement was for 25 °C and 45 °C data. For impedances estimated at 0 °C and 10 °C a 2nd order transfer function gave better fits than higher order models. As such the model order over all temperatures of interest is selected to equal two and the transfer function coefficients are estimated as a function of SoC and temperature.

Each estimated 2nd order transfer function can be used in subsequent simulations, however, if an ECM as shown in Figure 5 is required the transfer function is expanded via a partial fraction expansion to obtain the circuit parameters.

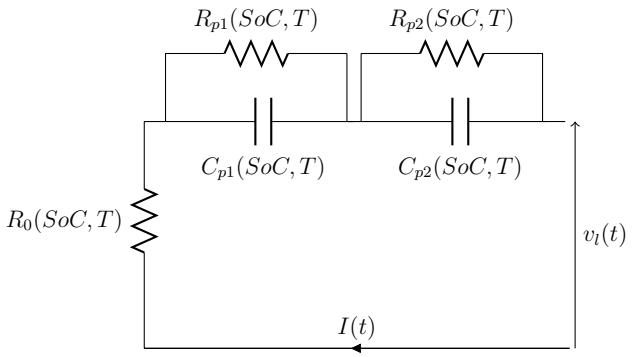

Figure 5: The 2nd order ECM structure used to represent the estimated transfer function. The OCV is not included since it is added at a later stage.

The partial fraction expansion of the 2nd order transfer function yields a direct term and two first order transfer functions of the form

$$Z_m(k) = -R_0 - \frac{R_{p1}}{\tau_1 j\omega_k + 1} - \frac{R_{p2}}{\tau_2 j\omega_k + 1} \tag{7}$$

where R_0 is assumed to represent the internal resistance, R_{p1} and R_{p2} the polarisation resistances and τ_1 and τ_2 the time constants. The Matlab®

function `residue` can be used to perform this expansion, whereby the transfer function coefficients $b_{nb}, \ldots, b_0, a_{nb-1}, a_0$ are passed as arguments and the function returns $-R_0$, the pole and gain of the two first order systems. The negative gain values then correspond to the polarisation resistances and the negative reciprocal of the poles to the time constants (equivalently the capacitances $C_{p1} = \tau_1/R_{p1}$ and $C_{p2} = \tau_2/R_{p2}$ are obtained).

3.2. Non-linear over-voltage function

The non-linear over-voltage function in the model (Figure 2) is motivated by the Tafel relation in electrochemical kinetics. As SoC and temperature decrease a higher over-potential is required to sustain a given current density. If the over-potential is sufficiently large the Butler-Volmer kinetics simplifies to the Tafel relation which is of the form

$$\eta = a + b \log i_d \tag{8}$$

where η is the over-potential (normally at a particular electrode), i_d is the current density and a and b are two constants.

Figure 6a shows a plot of the Tafel and Butler-Volmer kinetics relating an electrode over-potential to the current density. Mathematically, replacing the current density by any linear transformation will preserve the "S"-shape characteristic between the over-potential and transformed variable as shown in Figure 6b.

Given that the ECM is a linear model it linearly transforms an applied current $i(t)$ to a voltage $v_l(t)$ (see Figure 2). This voltage can be considered as the model over-voltage due to *linear* kinetic phenomena. Therefore, by plotting the *measured* over-voltage (equation (2)) against the *modelled* linear

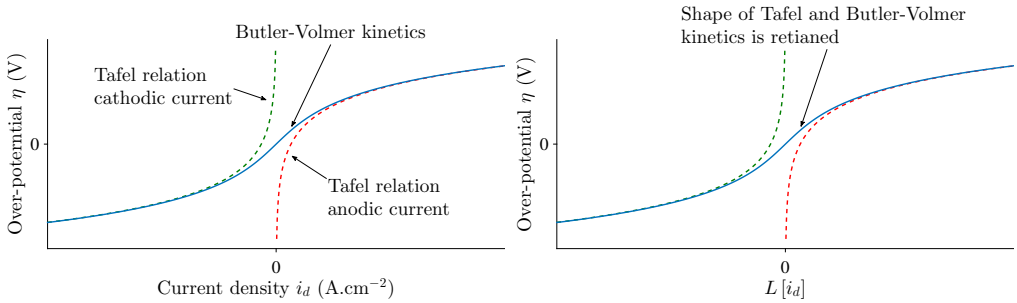

(a) A plot of the Tafel and Butler-Volmer kinetics

(b) A linear transform of the the current density preserves the shape

Figure 6: A linear transformation of the current density preserves the Tafel and Butler-Volmer shape.

over-voltage ($v_l(t)$), at each SoC and temperature, the presence of any non-linear deviations due to kinetic limitations can be examined and captured through a non-linear function.

To calculate $v_l(t)$ each of the designed pulse-mutisine signals ($i(n)$) is simulated with the corresponding estimated ECM to generate a linear over-voltage signal $v_l(n)$ and is denoted as

$$v_l(n) = \text{ECM}[i(n)] \quad n = 0, \ldots, NP-1 \tag{9}$$

To reduce the effects of transients the first period of $v_l(n)$ is discarded and the remaining $P-1$ periods are averaged to obtain the model linear over-voltage signal $\bar{v}_l(n)$ under steady-state conditions (equation 10).

$$\bar{v}_l(n) = \frac{1}{P-1}\sum_{p=2}^{P} v_l(N(p-1)+n) \quad n = 0, \ldots, N-1 \tag{10}$$

The measured over-voltage $\bar{v}_0(n)$ (equation 2) can now be plotted against the modelled linear over-voltage $\bar{v}_l(n)$ (equation 10) to investigate any non-linear

characteristics.

A plot of the measured vs modelled over-voltage when the battery is at 20 % SoC and 45 °C is shown in Figure 7a and the characteristic when the ambient temperature is at 0 °C is given in Figure 7b. While a strong linear

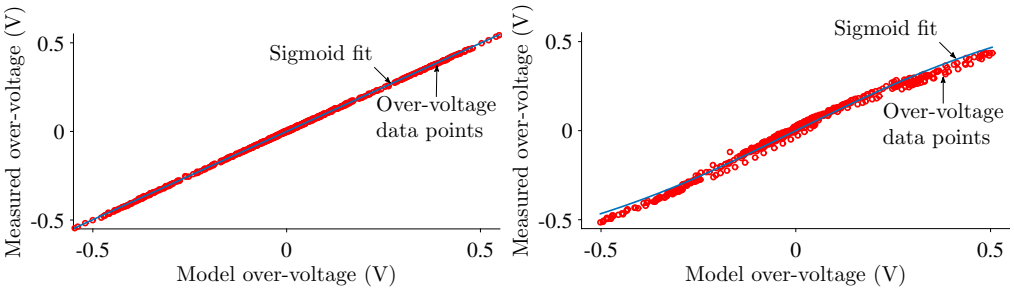

(a) Sigmoid function fit at 20 % SoC 45 °C (b) Sigmoid function fit at 20 % SoC 0 °C

Figure 7: The non-linear characteristic and sigmoid function fitting at 45 °C and 0 °C when at 20 % SoC of a 18650 Li-ion NCA battery. A non-linear behaviour is present at low SoC and low temperature.

dependence is observed when at 45 °C (Figure 7a) a non-linear deviation resembling that of a S-shape characteristic is observed when the battery is at 0 °C.

Such a characteristic can be modelled using a sigmoid function. Though the impact on modelling when choosing among the class of sigmoids is not studied here, to choose from a sigmoid class, as opposed to polynomials, is important as sigmoids are bounded, differentiable and if extrapolated the over-voltage will not diverge. Here, the following sigmoid function is used to fit the measured against modelled over-voltage data

$$f(\bar{v}_l) = \frac{c_1 \bar{v}_l}{\sqrt{1 + c_2 \bar{v}_l^2}} \tag{11}$$

while other possibilities include the logistic and hyperbolic tangent.

In equation (11) c_1 and c_2 are the sigmoid coefficients and need to be estimated. As $f(\bar{v}_l)$ is non-linear with respect to c_2 a non-linear optimisation routine is required to estimate c_1 and c_2 at each SoC and temperature. In this work the `lsqcurvefit` function from the Matlab® Optimsation Toolbox is used to perform the sigmoid function parameter estimation. The estimated coefficients are then tabulated in a linear look-up table for each SoC and temperature for model simulation.

3.3. OCV and hysteresis model block

The last block of the proposed Li-ion battery model structure (Figure 2) is the OCV and hysteresis block. One approach to estimate the open circuit voltage is to discharge and charge the battery with a low current (usually C/25), and average the measured charge and discharge voltages [5, 16, 17]. A low current is used to minimise any battery kinetics, however, even with a low discharge/charge current the battery will experience kinetic contributions when it is reaches complete discharge or charge leading to a high voltage drop; and the measured voltage can then no longer be assumed as the battery OCV.

In this work the method proposed in [18] is used to characterise OCV and hysteresis. The method involves discharging/charging the battery incrementally (e.g. at 4 % SoC intervals) followed by a rest period of 4 hours to allow the battery dynamics to relax and reach equilibrium. The voltage recorded from this method, also known as the incremental OCV method, better resembles the thermodynamic OCV estimate of the battery since the electrode kinetics are allowed to reach equilibrium.

To assess the magnitude of hysteresis incremental OCV tests are carried

out for discharging and charging a battery. The difference between the charge and discharge OCV curve is the battery hysteresis voltage. While lithium iron phosphate cathode batteries are known to exhibit hysteresis ([19, 20]), the work in [18] experimentally demonstrated the presence of a non-negligible level of hysteresis in other Li-ion systems. For the 3.03Ah $LiNiCoAlO_2$ batteries tested a 10-20 mV magnitude of hysteresis voltage is measured over 5 % - 95 % SoC. Following the details of [5] and [18], a first order transition model with regards to the SoC is then used to transit between the charge and discharge OCV curves.

Unlike the ECM and non-linear over voltage blocks, the OCV and hysteresis model block does not have any unknown parameters to be estimated. The model block is fully characterised though the incremental OCV tests.

4. Model Validation

A NL-ECM is estimated for each of the four tested 18650 Li-ion NCA batteries using the set of pulse-multisines as given in Appendix A. The mean and standard deviation of the estimated parameters R_0, R_{p1}, R_{p2}, τ_1, and τ_2 of the ECM (equation 7) and c_1 and c_2 of the non-linear over-voltage function (equation 11) are given in Table A.3.

Using the mean estimated parameters the NL-ECM model was validated with a drive-cycle current profile recorded from a prototype electric vehicle when driving in an urban environment with frequent accelerations and regenerative braking events (Figure 8a). The agreement between the measured and model voltage when at 70 % SoC and 10 °C and error are shown in Figure 8. The model root mean square error (RMSE) and peak error (pk-error)

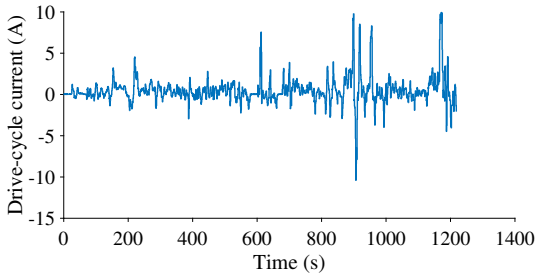

(a) Drive cycle current

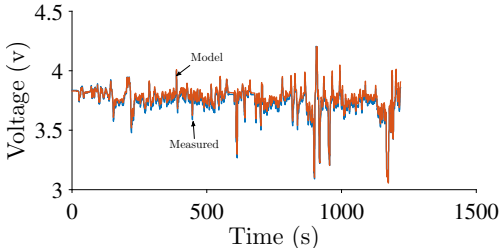

(b) Measured and NL-ECM model voltage

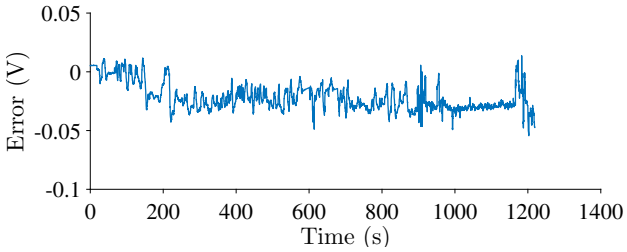

(c) Error

Figure 8: Validation profile and measured and model voltage at 70 % SoC 10 °C of a 18650 Li-ion NCA battery.

calculated over the drive-cycle currents applied at three conditions, 70 % 10 °C , 70 % 15 °C and 30 % 35 °C are given in Table 1.

In addition to the NL-ECM, a first-order linear ECM model was estimated using PPC test data at the same SoC and temperature points as the pulse-multisines. As shown in [2] a first-order ECM is sufficient to model pulse responses and as explained in the introduction the ECM is estimated as a function of SoC, temperature and current direction together with OCV with hysteresis. For comparison the two models are estimated at the same SoC and temperature points and are validated with the same drive-cycle current profiles. The RMSE and pk-error for the linear ECM is also given in Table 1.

	70 % SoC 10 °C		70 % SoC 15 °C		30 % SoC 35 °C	
	RMSE (V)	Pk Error (V)	RMSE (V)	Pk Error (V)	RMSE (V)	PK Error (V)
NL-ECM	2.49E-02	5.16E-02	2.75E-02	5.72E-02	1.18E-02	3.26E-02
Linear ECM	3.30E-02	1.35E-01	3.20E-02	1.20E-01	1.36E-02	6.74E-02
Reduction (%)	24.5%	61.6%	14.2%	52.4%	13.0%	51.6%

Table 1: RMSE and pk-error of the proposed model (NL-ECM) estimated using pulse-multisines and a first-order model (ECM) estimated with PPC tests. The NL-ECM gives consistently reduced RMSE and pk-error for the 18650 Li-ion NCA battery.

The results indicate that both the RMSE and pk-error of the NL-ECM improve when compared to the linear ECM by 13 % - 25 % and 52 % - 62 % respectively due to the estimated second order ECM and inclusion of a non-linear over-voltage function. The improvement of the RMSE and pk-error at lower temperature demonstrates that the effect of the non-linear over-voltage function is more prominent at lower temperatures. As the sigmoid function is linear at higher temperatures (Figure 7a) the reduction in RMSE and pk-error with increase in temperature is due to the second order ECM estimated based on the battery impedance.

5. Discussion

As a measure of model complexity it is worth comparing the number of model parameters of the NL-ECM to a linear ECM. The NL-ECM requires a total of seven parameters, with the second-order ECM consisting of five parameters and the non-linear over-voltage function consisting of two parameters. For the linear ECM, if a first-order ECM is estimated it will

require a total of six parameters, three parameters to represent discharge dynamics and three for the charge dynamics.

Though a linear ECM may seem a simpler model, due to one fewer parameter to estimate, it does not capture any non-linear dependence of the voltage on the current but only any dependence on the sign of the current, SoC and temperature. To further reduce a linear ECM's RMSE will require the use of a second-order ECM. Doing so will then increase the total number of model parameters to ten (five each for discharge and charge dynamics). As such the NL-ECM offers a good balance in model complexity while accounting for both charge and discharge dynamics and non-linearity without the need of a separate charge/discharge, or 3D, look-up table.

The 18650 Li-ion NCA batteries examined here are classed as energy batteries. It is worthwhile to further examine if the non-linear over-voltage function will show a stronger non-linear characteristic if higher currents than the recommended 10 s rating are used to drive such battery. Similarly, the level of non-linearity of Li-ion batteries optimised for power can also be examined. As such batteries are, however, designed to deliver high currents with low over-potentials, it is expected that the non-linear over-voltage function in the estimated NL-ECM model will be fairly linear even at low temperatures. This characteristic will be examined in further work.

6. Conclusions

The periodic and dynamic nature of a pulse-multisine signal enables the estimation of the impedance of a Li-ion battery and allows parametrisation over a broader bandwidth than a pulse signal. Furthermore, the large number

of signal amplitude levels allows any non-linearity from transport limitations at lower temperatures or SoCs to be characterised. By parametrising the non-linearity with a sigmoid function the proposed NL-ECM is a current dependent model without the need of a 3D look-up table for the model parameters.

The NL-ECM model of the 18650 Li-ion NCA battery resulted in a lower RMSE and pk-error (13 % - 25 % and 52 % - 62 % respectively) in comparison to the ECM estimated with PPC data. Including the non-linear over-voltage function improved both the RMSE and pk-error when operating below room temperature.

The impedance estimation of a battery via the LPM algorithm and non-linear over-voltage function estimation methodology is a general technique that can be used to model any Li-ion battery (high energy or power) dynamics and assess the level of non-linear behaviour. Part 1 [1] and Part 2 of this paper series presented a new signal design methodology (pulse-multisine), with a higher estimation bandwidth similar to a drive-cycle than a PPC test, and a new Li-ion model model structure (NL-ECM) with improved accuracy for use in BMS applications.

Acknowledgements

The research presented within this paper is supported by Innovate UK through the WMG centre High Value Manufacturing (HVM) Catapult in collaboration with Jaguar Land Rover and Tata Motors European Technical Centre.

Appendix A. Pulse-multisine design parameter settings and estimated Li-ion battery model parameters

	SoC				
	10 %	20 %	50 %	80 %	95 %
C_{dmax}	1	1.2	2	3	2
C_{cmax}	1.2	1.2	2	1.5	0.5
α	0.5	0.6	0.6	0.6	0.5
T_1	5	10	10	10	5
T_2	20	20	20	20	20
T_4	20	20	20	20	20
H_{exc}	1Hz	1Hz	1Hz	1Hz	1Hz

(a) For 0°C

	SoC				
	10 %	20 %	50 %	80 %	95 %
C_{dmax}	1.8	1.8	4	4	2
C_{cmax}	1.8	1.8	3	2	0.5
α	0.6	0.6	0.5	0.5	0.6
T_1	10	10	10	5	5
T_2	20	20	20	20	20
T_4	20	20	20	20	20
H_{exc}	1Hz	1Hz	1Hz	1Hz	1Hz

(b) For 10°C

	SoC				
	10 %	20 %	50 %	80 %	95 %
C_{dmax}	2	3.8	5.6	7	1.2
C_{cmax}	3	3.8	3	6.5	0.5
α	0.6	0.6	0.6	0.6	0.6
T_1	10	10	10	10	10
T_2	20	20	20	20	20
T_4	20	20	20	20	20
H_{exc}	1Hz	1Hz	1Hz	1Hz	1Hz

(c) For 25°C

	SoC				
	10 %	20 %	50 %	80 %	95 %
C_{dmax}	6	6	8	8	4
C_{cmax}	6	6	4	2	1
α	0.6	0.6	0.5	0.6	0.6
T_1	10	10	10	10	10
T_2	20	20	20	20	20
T_4	20	20	20	20	20
H_{exc}	1Hz	1Hz	1Hz	1Hz	1Hz

(d) For 45°C

Table A.2: Pulse-multisine design parameter values used for the 18650 Li-ion NCA battery model estimation.

SoC	R_o	Temperature 0 °C	10 °C	25 °C	45 °C
	10%	82.1 ± 1.3	45.6 ± 0.5	43.3 ± 0.7	32.9 ± 0.4
	20 %	82.6 ± 0.9	57.5 ± 0.4	42.6 ± 0.4	29.9 ± 0.4
	50 %	71.8 ± 0.7	48.6 ± 0.6	35.4 ± 0.4	27.3 ± 0.4
	80 %	63.1 ± 0.4	52.8 ± 0.7	35.8 ± 0.5	27.5 ± 0.4
	95 %	57 ± 5	44 ± 2	47.0 ± 0.4	31.2 ± 0.5

(a) Ohmic resistance R_o (mΩ)

SoC	R_{p1}	Temperature 0 °C	10 °C	25 °C	45 °C
	10 %	58.1 ± 1.2	29.7 ± 0.6	22.8 ± 0.4	1.945 ± 0.010
	20 %	67.9 ± 1.9	23.4 ± 1.1	3.9 ± 0.3	1.19 ± 0.02
	50 %	19.4 ± 0.7	4.51 ± 0.11	1.50 ± 0.04	1.45 ± 0.07
	80 %	18.1 ± 0.9	5.73 ± 0.13	1.60 ± 0.02	1.26 ± 0.03
	95 %	55 ± 5	32 ± 3	6.4 ± 0.6	1.6 ± 0.2

(b) Polarisation resistance R_{p1} (mΩ)

SoC	R_{p2}	Temperature 0 °C	10 °C	25 °C	45 °C
	10 %	118 ± 3	69 ± 3	28.9 ± 1.0	14.6 ± 0.3
	20 %	55.1 ± 1.4	22.6 ± 0.3	18.8 ± 0.3	11.91 ± 0.13
	50 %	35.3 ± 1.3	20.1 ± 0.3	15.4 ± 0.2	9.98 ± 0.15
	80 %	32.5 ± 0.3	28.4 ± 0.5	15.5 ± 0.2	9.1 ± 0.4
	95 %	39.6 ± 0.7	26.2 ± 0.3	18.5 ± 1.1	11.1 ± 0.9

(c) Polarisation resistance R_{p2} (mΩ)

SoC	τ_1	Temperature 0 °C	10 °C	25 °C	45 °C
	10 %	0.45 ± 0.02	0.147 ± 0.003	0.265 ± 0.008	0.41 ± 0.02
	20 %	0.526 ± 0.004	0.228 ± 0.006	0.239 ± 0.005	0.80 ± 0.02
	50 %	0.228 ± 0.003	0.203 ± 0.006	0.90 ± 0.02	0.76 ± 0.10
	80 %	0.18 ± 0.02	0.226 ± 0.005	0.45 ± 0.02	0.70 ± 0.04
	95 %	0.126 ± 0.016	0.102 ± 0.008	0.19 ± 0.03	1.1 ± 0.4

(d) Time constant τ_1 (s)

SoC	τ_2	Temperature 0 °C	10 °C	25 °C	45 °C
	10 %	4.4 ± 0.2	7.0 ± 0.2	12.3 ± 0.3	16.1 ± 0.7
	20 %	29.8 ± 0.10	16.8 ± 0.2	19.8 ± 0.3	16.8 ± 0.2
	50 %	29.1 ± 1.1	21.0 ± 0.4	23.6 ± 0.4	18.6 ± 1.0
	80 %	23.7 ± 0.3	20.3 ± 0.5	18.5 ± 0.2	10.9 ± 0.6
	95 %	7.4 ± 0.4	16.5 ± 0.8	16.5 ± 1.8	14 ± 3

(e) Time constant τ_2 (s)

SoC	c_1	Temperature 0 °C	10 °C	25 °C	45 °C
	10 %	1.090 ± 0.005	1.374 ± 0.005	1.167 ± 0.002	0.9939 ± 0.0012
	20 %	1.072 ± 0.004	1.052 ± 0.003	1.020 ± 0.002	0.9978 ± 0.0008
	50 %	1.045 ± 0.004	1.0015 ± 0.0009	0.997 ± 0.0003	0.9896 ± 0.0016
	80 %	1.0076 ± 0.0004	1.000 ± 0.002	0.9968 ± 0.0009	0.9711 ± 0.0015
	95 %	1.092 ± 0.006	1.0142 ± 0.0014	0.984 ± 0.005	0.980 ± 0.005

(f) Sigmoid coefficient c_1

SoC	c_2	Temperature 0 °C	10 °C	25 °C	45 °C
	10 %	3.11 ± 0.08	2.90 ± 0.06	3.39 ± 0.04	0.003 ± 0.002
	20 %	1.32 ± 0.03	1.20 ± 0.05	0.30 ± 0.03	0.011 ± 0.009
	50 %	1.27 ± 0.07	0.046 ± 0.013	(0.5 ± 0.2)× 1e-6	(0.48 ± 0.14)× 1e-7
	80 %	0.080 ± 0.004	0.077 ± 0.013	(0.6 ± 0.4)× 1e-8	(0.06 ± 0.10)× 1e-8
	95 %	0.55 ± 0.03	0.14 ± 0.03	0.002 ± 0.004	(2.7 ± 0.7)× 1e-6

(g) Sigmoid coefficient c_2

Table A.3: The mean and standard deviation of the estimated ECM and non-linear over-voltage function coefficients of the NL-ECM model based on the four 18650 Li-ion NCA batteries.

Appendix B. Local Polynomial Method to estimate battery impedance

In LPM $Z(k)$ is approximated via a low degree polynomial in the neighbourhood of k as

$$Z(k+r) = Z(k) + \sum_{s=1}^{S} r^s z_s(k) + R_Z \qquad \lim_{S\to\infty} R_Z = 0 \tag{B.1}$$

In equation (B.1) S is the degree of the polynomial, R_Z is the remainder and the polynomial variable r is the harmonic number relative to k. The voltage at harmonic $k+r$ can be expressed as

$$V(k+r) = Z(k+r)I(k+r) + E(k+r) \tag{B.2}$$

Substituting for $Z(k+r)$ (equation (B.1)) into equation (B.2) results in a function where the unknown parameters occur linearly. These unknown parameters are $Z(k)$ and the polynomial coefficients, $z_1, \ldots, z_S$.

By setting $r = -R, \ldots, 0, \ldots, R$, which defines a narrow frequency window around the k^{th} harmonic, a system of linear equations is obtained. This can be written in a compact matrix form as

$$\boldsymbol{V} = \boldsymbol{K}\boldsymbol{\theta} + \boldsymbol{E} \tag{B.3}$$

where in equation (B.3) $\boldsymbol{V} = [V(k-R), \ldots, V(k+R)]'$ is a $\mathbb{C}^{2R+1}$ vector of the voltages around harmonic k, $\boldsymbol{K} \in \mathbb{C}^{(2R+1)\times(S+1)}$ is the regressor matrix, with each row of $\boldsymbol{K}$ being $I(k+r)[1, r, \ldots, r^S]$, $\boldsymbol{\theta} = [Z(k), z_1(k), \ldots, z_S(k)]'$ is the unknown parameter vector and $\boldsymbol{E} \in \mathbb{C}^{2R+1}$ is a vector of errors.

By ensuring that $R > S/2$ an estimate of the parameters ($\hat{\boldsymbol{\theta}}$), and hence an estimate of the impedance ($\hat{Z}(k)$), and its variance ($\sigma^2_{\hat{Z}}(k)$) can be obtained via the linear least squares method [21] as

$$\hat{\boldsymbol{\theta}} = (\boldsymbol{K}^{\boldsymbol{H}}\boldsymbol{K})^{-1}\boldsymbol{K}^{\boldsymbol{H}}\boldsymbol{V} \tag{B.4}$$

and superscript H is the conjugate transpose. The covariance matrix ($\boldsymbol{C}_{\hat{\boldsymbol{\theta}}}$) of the parameters is calculated through the residual vector $\boldsymbol{Q}$ as $\boldsymbol{Q} = \boldsymbol{V} - \boldsymbol{K}\hat{\boldsymbol{\theta}}$, $\boldsymbol{C}_{\hat{\boldsymbol{\theta}}}$ is then [21]

$$\boldsymbol{C}_{\hat{\boldsymbol{\theta}}} = (\boldsymbol{K}^{\boldsymbol{H}}\boldsymbol{K})^{-1}\boldsymbol{Q}^{\boldsymbol{H}}\boldsymbol{Q}/d \tag{B.5}$$

where each diagonal entry of $\boldsymbol{C}_{\hat{\boldsymbol{\theta}}}$ is the variance estimate of the corresponding parameter. In equation (B.5) d is the difference between the number of harmonics over which the polynomial is fitted and the number of parameters and simplifies to $d = 2R - S$. In this work the polynomial order is set to $S = 2$ and a frequency window with $R = 2$ is used. For any interested person, the LPM algorithm is available to download as a Matlab function from the following Github repository `https://github.com/WDWidanage/MatlabFunctions/`.

References

[1] W. Widanage, A. Barai, G. Chouchelamane, K. Uddin, A. McGordon, J. Marco, P. Jennings, Design and use of multisine signals for Li-ion battery equivalent circuit modelling. Part 2: Model estimation, Journal of Power Sources 324 (-) (2016) 61–69. doi:10.1016/j.jpowsour.2016.05.014.
URL http://dx.doi.org/10.1016/j.jpowsour.2016.05.015http://linkinghub.elsevier.com/retrieve/pii/S037877531630550X

[2] X. Hu, S. Li, H. Peng, A comparative study of equivalent circuit models for li-ion batteries, Journal of Power Sources 198 (2012) 359–367.

[3] M. Dubarry, B. Y. Liaw, Development of a universal modeling tool for rechargeable lithium batteries, Journal of Power Sources 174 (2) (2007) 856–860. doi:10.1016/j.jpowsour.2007.06.157.

[4] B. Y. Liaw, G. Nagasubramanian, R. G. Jungst, D. H. Doughty, Modeling of lithium ion cells-A simple equivalent-circuit model approach, Solid State Ionics 175 (1-4) (2004) 835–839. doi:10.1016/j.ssi.2004.09.049.
URL http://linkinghub.elsevier.com/retrieve/pii/S0167-2738(04)00667-8

[5] G. L. Plett, Extended kalman filtering for battery management systems of LiPB-based HEV battery packs: Part 2. Modeling and identification, Journal of power sources 134 (2) (2004) 262–276.

[6] K. Uddin, A. Picarelli, C. Lyness, N. Taylor, J. Marco, An Acausal Li-Ion Battery Pack Model for Automotive Applications, Energies 7 (9) (2014) 5675–5700. doi:10.3390/en7095675.
URL http://www.mdpi.com/1996-1073/7/9/5675/

[7] L. Ménard, G. Fontès, S. Astier, Dynamic energy model of a lithium-ion battery, Mathematics and Computers in Simulation 81 (2) (2010) 327–339. doi:10.1016/j.matcom.2010.07.026.
URL http://linkinghub.elsevier.com/retrieve/pii/S0378475410002636

[8] A. Jossen, Fundamentals of battery dynamics, Journal of Power Sources 154 (2) (2006) 530–538. doi:10.1016/j.jpowsour.2005.10.041.
URL http://linkinghub.elsevier.com/retrieve/pii/S0378775305014321

[9] S. Yuan, H. Wu, C. Yin, State of charge estimation using the extended kalman filter for battery management systems based on the arx battery model, Energies 6 (1) (2013) 444–470.

[10] T. Huria, M. Ceraolo, J. Gazzarri, R. Jackey, High fidelity electrical model with thermal dependence for characterization and simulation of high power lithium battery cells, in: Electric Vehicle Conference (IEVC), 2012 IEEE International, IEEE, 2012, pp. 1–8.

[11] C. Birkl, D. Howey, Model identification and parameter estimation for lifepo4 batteries, in: IET Hybrid and Electric Vehicles Conference 2013 (HEVC 2013), London, UK, 2013, pp. 1764–1769.

[12] C. Antaloae, J. Marco, F. Assadian, A novel method for the parameterization of a li-ion cell model for EV/HEV control applications, IEEE Transactions on Vehicular Technology 61 (9) (2012) 3881–3892.
URL http://ieeexplore.ieee.org/xpls/abs{_}all.jsp?arnumber=6270007

[13] N. Omar, Ph.D. Thesis: Assessment of Rechargeable Energy Storage Systems for Plug-In Hybrid Electric Vehicles, VUBPRESS Brussels University Press, 2012.

[14] R. Pintelon, J. Schoukens, G. Vandersteen, K. Barbe, Estimation of nonparametric noise and FRF models for multivariable systems- part I: Theory, Mechanical Systems and Signal Processing 24 (3) (2010) 573–595.

[15] I. Kollár, Frequency Domain System Identification Toolbox for Matlab, Budapest, 2004-2014.

[16] B. Pattipati, B. Balasingam, G. Avvari, K. Pattipati, Y. Bar-Shalom, Open Circuit Voltage Characterization of Lithium-ion Batteries, Journal of Power Sources 269 (2014) 317–333. doi:10.1016/j.jpowsour.2014.06.152.
URL http://www.sciencedirect.com/science/article/pii/S037877531401026X

[17] V. Pop, H. J. Bergveld, J. H. G. Op het Veld, P. P. L. Regtien, D. Danilov, P. H. L. Notten, Modeling Battery Behavior for Accurate State-of-Charge Indication, Journal of The Electrochemical Society

153 (11) (2006) A2013. doi:10.1149/1.2335951.
URL http://jes.ecsdl.org/cgi/doi/10.1149/1.2335951

[18] A. Barai, W. D. Widanage, J. Marco, A. McGordon, P. Jennings, A study of the open circuit voltage characterization technique and hysteresis assessment of lithium-ion cells, Journal of Power Sources 295 (2015) 99–107. doi:10.1016/j.jpowsour.2015.06.140.
URL http://linkinghub.elsevier.com/retrieve/pii/S037877531530029X

[19] W. Dreyer, J. Jamnik, C. Guhlke, R. Huth, J. Moškon, M. Gaberšček, The thermodynamic origin of hysteresis in insertion batteries, Nature Materials 9 (5) (2010) 448–453. doi:10.1038/nmat2730.
URL http://www.nature.com/doifinder/10.1038/nmat2730

[20] V. Srinivasan, J. Newman, Existence of Path-Dependence in the LiFePO[sub 4] Electrode, Electrochemical and Solid-State Letters 9 (3) (2006) A110. doi:10.1149/1.2159299.

[21] J. V. Beck, K. J. Arnold, Parameter Estimation In Engineering and Science, Wiley, NY, 1977.